Nanoscale Origin of Mesoscale Roughening: Real-Time Tracking and Identification of Three Distinct Ruthenium Oxide Phases in Ruthenium Oxidation

Jan Ingo Flege,*,† Benjamin Herd,‡ Jan Goritzka,‡ Herbert Over,‡ Eugene E. Krasovskii,§,⊥,∥ and Jens Falta†,#

†Institute of Solid State Physics, University of Bremen, Otto-Hahn-Allee 1, 28359 Bremen, Germany, ‡Department of Physical Chemistry, Justus-Liebig-University, Heinrich-Buff-Ring 58, 35392 Gießen, Germany, §Departamento de Física de Materiales, Universidad del Pais Vasco UPV/EHU, 20080 San Sebastián/Donostia, Basque Country, Spain, ⊥Donostia International Physics Center (DIPC), 20018 San Sebastián/Donostia, Basque Country, Spain, ∥IKERBASQUE, Basque Foundation for Science, 48011 Bilbao, Spain, and #MAPEX Center for Materials and Processes, University of Bremen, 28359 Bremen, Germany

ABSTRACT The structural modification of the Ru(0001) surface is followed *in real-time* using low-energy electron microscopy at elevated temperatures during exposure to molecular oxygen. We observe the nucleation and growth of three different RuO_2 facets, which are unambiguously identified by single-domain microspot low-energy electron diffraction (μLEED) analysis from regions of 250 nm in diameter. Structural identification is then pushed to the true nanoscale by employing very-low-energy electron reflectivity spectra $R(E)$ from regions down to 10 nm for structural fingerprinting of complex reactions such as the oxidation of metal surfaces. Calculations of $R(E)$ with an *ab initio* scattering theory confirm the growth of (110), (100), and (101) orientations of RuO_2 and explain the shape of the $R(E)$ spectra in terms of the conducting band structure. This methodology is ideally suited to identify the structure of supported ultrathin films and dynamic transformations at multicomponent interfaces down to few nanometer lateral resolution at elevated temperature and in reactive environments.

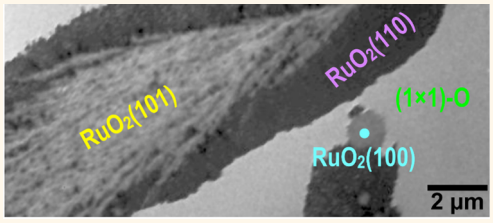

KEYWORDS: ruthenium · low-energy electron microscopy and diffraction · transition metal oxidation · *in situ* methods · augmented plane wave method

Oxidation is an almost ubiquitous phenomenon and is typically observed when metals are exposed to an oxygen-rich environment. Fundamentally, the oxidation of metal surfaces represents a remarkably complex reaction scenario at the solid−gas interface, in which heterogeneities at the surface as well as the supply and transport of the reacting surface species are decisive ingredients.[1] In the course of metal oxide formation, the metal−metal bonding is replaced by metal−oxygen bonding, a process which is thermally activated and therefore may be rate-determining at low temperatures. Assuming a nucleation and growth type mechanism, the kinetics of surface oxidation is dictated by both the supply of mobile metal atoms, which have to be detached from the metallic network, and by the atomic surface oxygen species, which need to be formed by dissociation of molecular oxygen from the gas phase. Both kinetic constraints require elevated temperatures and, in particular, higher oxygen pressures during the oxidation of the metal surface, with the exact conditions depending on the material.[1−3]

Even if the initial processes in the oxidation of a metal surface are well understood on the microscopic level, the further growth of the oxide is frequently accompanied by a substantial roughening and patterning of the surface at the mesoscale, whose physical and chemical origin is far less understood. For metals that are able to form several stable oxides, as, *e.g.*, Fe, the coexistence of different oxides can be observed on the surface.[4−6] To gain mesoscale information on the oxidation of the metal surface, we need to apply an *in situ* technique

* Address correspondence to flege@ifp.uni-bremen.de.

Received for review June 4, 2015 and accepted July 14, 2015.

Published online July 14, 2015
10.1021/acsnano.5b03393

that is able to discriminate various oxides or oxide orientations under real-time oxidation conditions with a spatial resolution of some 10 nm.

Here, we will focus on the oxidation of single crystalline Ru(0001) surface with molecular oxygen. Recent studies on this system have initiated a paradigm shift in catalysis research by establishing the notion that oxides can be more active than the corresponding metal catalysts.[7] Ruthenium forms only a single solid oxide, namely RuO_2, so that the oxidation behavior on the mesoscale is simpler than in other cases of multiple cation valency, yet still lacking a coherent picture and a detailed relation to the processes occurring at the atomic scale. Above temperatures of 550 K, the initial oxidation of Ru(0001) has been shown by scanning tunneling microscopy (STM) to proceed *via* a modified nucleation and growth mechanism.[8] Three-dimensional RuO_2 domains (clusters) are exclusively formed at double steps of Ru(0001). Upon further oxygen exposure, most of these clusters grow slowly in size, but only very few of them are able to initiate the fast growth of atomically flat RuO_2 domains with their (110) face oriented along the [0001] direction of the Ru substrate. However, closer inspection of the available STM images[7] in the literature reveals the presence of other presumedly oxidic, yet unknown, surface components that seem to coexist with the established RuO_2(110) phase, rendering the oxidation of the Ru(0001) system more complex than frequently anticipated.

The oxidation of Ru(0001) with molecular oxygen at elevated temperatures was already examined on the mesoscale by photoelectron emission microscopy (PEEM)[9] and scanning photoemission microscopy (SPEM).[10−12] These studies indicated that the transition from oxygen adsorption to oxide formation is structurally and morphologically intricate, with complex pattern formation on the Ru(0001) surface, revealing surface features of lateral dimensions on the nanometer or even micrometer scale. Yet, firm conclusions could not be drawn from these data since both techniques lack the required structural sensitivity: On the one hand, PEEM does not provide any chemical or structural information (the contrast is due to local variations of the work function), while on the other hand, *ex situ* SPEM can discriminate between RuO_2 and adsorbed oxygen, however, without supplying sufficient information to explain the observed contrast variation in the RuO_2 regions.

Here, we study *in situ* the oxidation of Ru(0001) by molecular oxygen at higher sample temperatures with low energy electron microscopy (LEEM). We use this complex interfacial reaction in a *proof-of-principle* fashion to illustrate the unprecedented capabilities of *in situ* intensity−voltage (*I*(*V*)) LEEM for real-time structural identification in reactive environments when combined with state-of-the-art modeling within the framework of *ab initio* scattering theory. This approach, employing a nondestructive laboratory method, allows mapping the mesoscale surface morphology with structural sensitivity on the few nanometer scale. We show that the observed patterning of the oxide surface is due to the nanoscale coexistence of RuO_2 grains of various orientations on the Ru(0001) surface. By virtue of our *in situ* method, we are also able to demonstrate that the RuO_2(100) phase, a phase thought to be least stable thermodynamically, grows first and then fosters the nucleation of other faces of RuO_2.

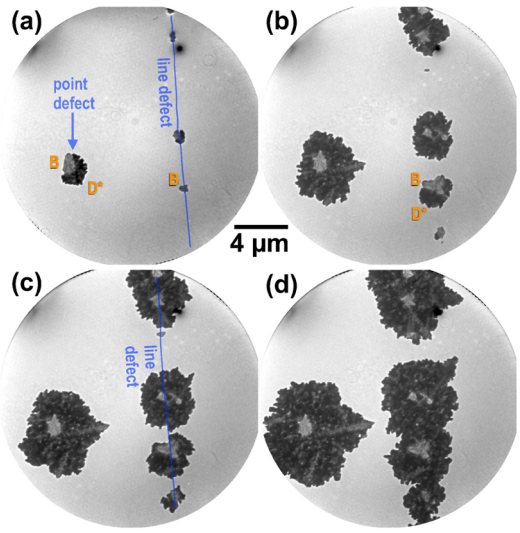

Figure 1. LEEM (electron kinetic energy: 8.4 eV) time-lapse sequence showing the oxidation of the Ru(0001) surface by exposure to O_2 at temperature T = 780 K and $p(O_2) = 3 \times 10^{-5}$ Torr. The O_2 dose is (a) 36.8 kL, (b) 64.0 kL, (c) 77.6 kL, and (d) 101.3 kL. The bright phase "B" nucleates before the dark phase "D*" next to "B".

RESULTS AND DISCUSSION

***In Situ* LEEM Imaging of Ru(0001) Oxidation.** We follow *in situ* the oxidation of a Ru(0001) crystal during the exposure to molecular oxygen at a sample temperature of 780 K. The respective time-lapse LEEM image sequence is displayed in Figure 1. After a dose of about 37 kL, small oxide domains have nucleated at line- and point-like surface defects with low nucleation density [Figure 1a]. These islands eventually grow upon further oxygen exposure at the expense of the chemisorbed oxygen layer, see Figure 1b−d and Supporting Information Movie S1.

It is interesting to note that the growing oxide islands exhibit a complex internal structure (contrast variation), *i.e.*, they consist of a multitude of very small, apparently distinct oxide domains that often measure less than a hundred nanometers in diameter. Close inspection reveals that the bright phase "B" nucleates first and directly at the defect site, while the darker, seemingly inhomogeneous patches "D*" only form during a secondary nucleation process occurring next to the primary nuclei "B" at later stages [Figures 1b,c]. Together, these effects give rise to a complex "mosaic-like"

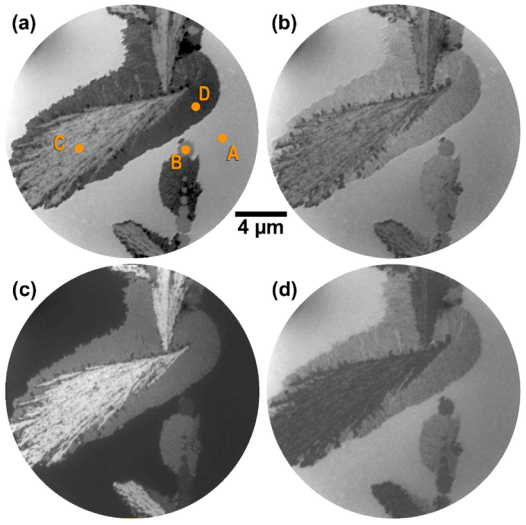

Figure 2. LEEM still images recorded after oxidation at 680 K and $p(O_2) = 3 \times 10^{-5}$ Torr. Electron energies are (a) 9.5 eV, (b) 13.1 eV, (c) $E = 16.9$ eV, and (d) 38.8 eV. Filled circles in (a) demark the positions where μLEED images and $I(V)$ curves have been analyzed.

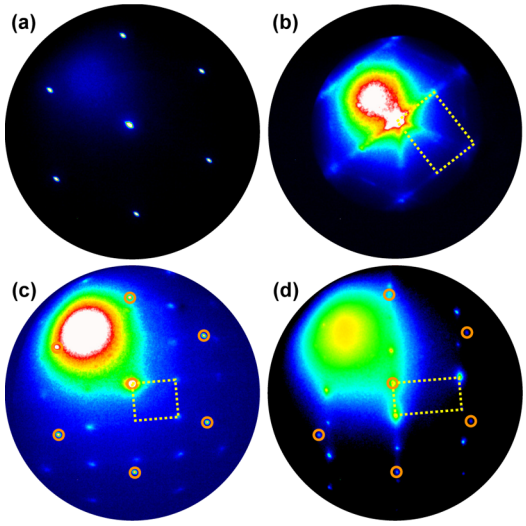

Figure 3. Microspot (250 nm) LEED patterns obtained after oxidation of the Ru(0001) surface by exposure to 72 kL of O_2 at a substrate temperature $T = 680$ K. The reflections of the (1×1)-ordered substrate (a) are also highlighted in (c) and (d) and have been used for reciprocal space calibration. The unit mesh is indicated in all RuO_2 patterns. The images show single-domain patterns of (b) RuO_2(100) ($E = 29.0$ eV, near grain boundary), (c) RuO_2(101) ($E = 56.5$ eV), and (d) RuO_2-(110) ($E = 56.5$ eV).

appearance of the emerging oxide "film", with the primary phase "B" assembled like "beads on a string" at the center of the coalescing oxide patches [Figure 1d].

The finding of a multicomponent, heterogeneous surface is confirmed by oxidizing the Ru(0001) surface at a lower temperature of 680 K, which apparently leads to the formation of larger oxide grains. This is demonstrated by the series of LEEM images displayed in Figure 2, which were recorded after exposing the Ru(0001) surface to 72 kL of O_2 at a partial pressure of 3×10^{-5} Torr. Clearly, the contrast varies strongly with the electron kinetic energy, revealing an internal structure of the oxide islands at a larger length scale than found at 780 K [Figure 1d].

Although the islands of phase "B" still nucleate first and still preferentially form along line defects (see Figure 2a), the oxide growth is found to be more anisotropic than at 780 K. Also, it is now clear that the dark patches "D*" previously observed at 780 K consist of at least two extended phases labeled "C" and "D".

Micro-Diffraction Analysis. Phase-specific μLEED patterns of the predominant surface phases besides the coexisting (1×1)-O chemisorbed phase have been recorded at positions as labeled in Figure 2a and are displayed in Figure 3b–d along with the respective unit mesh for each oxide structure. Using the (1×1)-O LEED pattern (Figure 3a) for the calibration of reciprocal space, the respective unit mesh dimensions of the individual phases can be determined. The results are compiled in Table 1.

From the respective unit mesh geometries, all phases are identified as specific faces of RuO_2, each exhibiting a (1×1) periodicity. The experimentally determined lattice constants lie very close to or even are within the error bar of the bulk values expected for a particular facet, and the orientation of the islands are azimuthally well-defined with respect to the Ru(0001) substrate. The remaining (small) difference is attributed to residual strain in the thin oxide layers. While finding the well-characterized RuO_2(110) phase is expected,[1] the occurrence of flat RuO_2(100) and RuO_2-(101) phases after oxidation of the Ru(0001) surface has not been reported yet and is surprising.

TABLE 1. Experimental In-Plane Lattice Constants (Uncertainty: (0.03–0.05) Å) and Respective Bulk Values[1] Determined by Kinematical Analysis for the Local LEED Patterns Acquired from Different RuO_2 Crystallographic Faces (Figure 3)

	experimental	reference
face	lattice constant (Å)	bulk value (Å)
(110)	3.10	3.11
	6.40	6.35
(101)	4.57	4.49
	5.47	5.46
(100)	3.07	3.11
	4.51	4.49

It should be noted that the average domain size of the (100) phase is very small, which makes it virtually impossible to record single domains LEED patterns on a length scale of 250 nm as defined by our smallest illumination aperture. In contrast, the RuO_2(110) phase exhibits the sharpest LEED spots, indicative of well-ordered single-crystalline domains. From the simultaneous observation of the substrate LEED spots and the (110) and (101) oxide reflections in μLEED, we can estimate the respective oxide thicknesses to be lower

than 1−1.5 nm, which is consistent with the results of a previous surface X-ray diffraction study for RuO_2(110).[13] As we only detect very weak traces of the substrate (if any) in all collected μLEED patterns of the (100) orientation for electron kinetic energies between 15 and 60 eV, these domains must be significantly thicker.

Identifying Individual Nanoscale Oxide Grains by *I*(*V*)-LEEM. Due to the small oxide grain size at even higher temperatures (*cf.* Figure 1d), which prevents the recording of single-phase LEED patterns, clearly another means of phase or face identification on the few nanometer scale is needed. Here, we will demonstrate that this goal, and specifically the identification of individual oxide faces, can be achieved by recording local *I*(*V*) curves in the VLEED regime with a lateral resolution of about 10 nm, which facilitates direct identification in real space and which is equivalent to an improvement in lateral resolution by a factor higher than 20.

Representative *I*(*V*) curves for the different crystallographic orientations of RuO_2 and the (1 × 1)-O adlayer phase are compared in Figure 4a. Evidently, all *I*(*V*) curves exhibit a characteristic shape and are sufficiently different to enable unambiguous identification of the local nanoscale oxide structure.

To be able to identify the complicated multicomponent surface presented in Figure 4b,c based on the *I*(*V*) curves, we must be confident that they do characterize RuO_2 crystal faces, and that the specific shape of the curves is not caused by any extrinsic factors. Our identification is corroborated by the comparison in Figure 4a of the measured curves with the *ab initio* *R*(*E*) spectra for the three RuO_2 orientations: RuO_2(110), RuO_2(101), and RuO_2(100). Generally, the calculated curves are in a good agreement with the measurements despite the assumption of a bulk-like oxide structure, which is an approximation because of the presence of residual strain and the typical self-terminating oxide layer thickness in the few nanometer range.[13] The comparison is less perfect for the (100) surface, which is presumably explained by the weaker signal from the (100) species. Nevertheless, also in this case the gross features of the spectrum are well reproduced.[15] Thus, the present theory unambiguously relates the very different shape of the curves to the electronic structure of differently orientated RuO_2 crystallites and suggests that the surface layer is not compositionally different from the bulk.

Finally, we apply the *I*(*V*)-LEEM approach to the local identification of the individual components of the complex multicomponent oxide structures evolving at temperatures of 680 and 780 K (*cf.* Figures 2, 4b-c, and Supporting Information Movie S1). On the basis of local *I*(*V*) analysis after suitably correcting for image drift, we may associate each portion of the image with a distinct oxygen-rich phase by comparing with the representative *I*(*V*) curve from our "*I*(*V*) catalog" shown

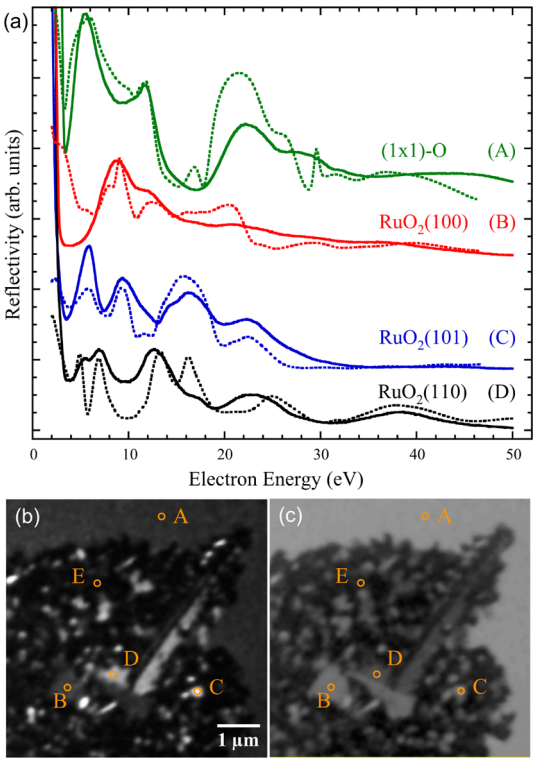

Figure 4. (a) Compilation of representative very-low-energy electron reflectivity spectra (solid lines) obtained after oxidation of the Ru(0001) surface by exposure to O_2 at $p(O_2)$ = 3 × 10^{-5} Torr and various substrate temperatures between 600 and 780 K as well as comparison to calculated normal-incidence reflectivity spectra (dashed lines) based on *ab initio* scattering theory. The calculated spectrum for the (1 × 1)-O adlayer is taken from previous work.[14] (b and c) LEEM images recorded after oxidation of the Ru(0001) surface by exposure to O_2 at $p(O_2)$ = 3 × 10^{-5} Torr at 780 K substrate temperature. The energies are (b) 14.7 eV and (c) 10.4 eV. The following nanoscale phases are identified: (A) (1 × 1)-O, (B) RuO_2(100), (C) RuO_2(101), (D) RuO_2(110), and (E) disordered/mixed oxide grains. In (c), the grayscale has been adjusted to enhance contrast.

in Figure 4a. At both temperatures, three unique crystallographic phases of RuO_2 have grown at the expense of the (1 × 1)-O chemisorbed phase. Furthermore, as previously discussed, at 780 K it is clearly visible that the (100) phase preferentially nucleates first; then, these patches subsequently act as a secondary nucleation sites for the other phases (also see Supporting Information Movie S1). This finding is contrary to the expectations based on the relative thermodynamic stabilities of the different faces of RuO_2, which would essentially dictate the prevalence of the (110) orientation followed by the (101) and finally the (100) orientation.[16,17]

Despite its higher surface free energy, the preference for the RuO_2(100) phase at the initial stage of nucleation may be rationalized by considering its superior epitaxial lattice matching to the Ru(0001) template as compared to the (110) orientation. While the translation vectors of the surface unit cells along the [001] directions of the RuO_2(100) and RuO_2(110)

structures, *i.e.*, along the $\langle 2\bar{1}\bar{1}0\rangle$ high symmetry directions of the substrate, share the same length (3.11 Å), the length of the [010] unit vector (4.49 Å) of the RuO_2(100) phase is close to two times the row spacing (4.69 Å) of the Ru(0001) template along the $\langle 01\bar{1}0\rangle$ direction, whereas the epitaxial misfit of the RuO_2(110) phase in the same direction is larger.[18] Hence, this similarity in lattice constants may trigger the formation of a strained coincidence lattice at the metal−oxide interface, apparently rendering the (100) orientation the thermodynamically most stable RuO_2 phase for sufficiently thin oxide layers. Yet, a gradual thickening of the oxide would steadily increase the amount of strain energy that cannot be counterbalanced by the gain in interfacial energy, resulting in both strain release of the RuO_2(100) islands concomitant with adjacent nucleation of the (110) phase. Consequently, this scenario may explain both the finding of a critical thickness and a finite lateral extent of the (100) phase, which may depend on temperature.

Although we do not have any direct experimental evidence for the formation of a coincidence lattice, its existence would also help to explain why the (100) phase is favored in electrochemical oxidation of Ru(0001),[19] which is a process strongly driven by kinetics. Furthermore, it should be noted that the growth of the rutile (100) phase has also been confirmed[20,21] for gas-phase oxidation of Ir(111), a related transition metal with similar lattice constants. Interestingly, while the growth of IrO_2(100) is found to compete with concomitant growth of corundum-like Ir_2O_3(0001), no indication for the analoguous growth of a hexagonal Ru_2O_3(0001) oxide has been observed yet.

As the relative surface coverage of the individual phases also seems to depend on temperature, together with the initial preferential growth of the (100) orientation these effects lead to a scenario where the nucleation density, *i.e.*, the nanoscale heterogeneity is not simply related to the growth temperature in an Arrhenius-like fashion. Also, especially at 780 K, a considerable fraction of the surface is covered by a phase that exhibits a very low electron reflectivity ("dark patches"), whose *I*(*V*) spectra mostly resemble the (1 × 1)-O phase. Therefore, this nanoscale multigrain morphology comprises both ordered and disordered oxide nuclei, and it remains stable throughout the oxidation process. These observations provide strong evidence for the notion that this stage of the oxidation process, which is highly influenced by the initial morphology of the Ru metal and driven by the metal−oxide interfacial interaction, is crucial in defining the final metal/oxide mesoscale surface and interface structure. Furthermore, these observations also provide a handle on how to tailor the oxide morphology and composition by deliberate patterning of the substrate or employing vicinal surfaces.

CONCLUSION

We have presented an *in situ* structural study of the oxidation of the Ru(0001) surface during exposure to molecular oxygen at elevated temperature, revealing a complex morphology consisting of various oxide components with morphological variations on nanoscopic to mesoscopic length scales depending on substrate temperature. Using a combination of LEEM and μLEED, we have identified the main emerging ruthenium oxide phases as the (110), (100), and (101) orientations of RuO_2, which concurrently evolve at the expense of the chemisorbed oxygen adlayer phase. All surface phases identified by μLEED exhibit distinct electron reflectivity spectra, establishing a clear one-to-one correspondence between the contrast in LEEM and the local atomic structure. By comparing to *ab initio* calculations of electron scattering from crystalline surfaces, the pronounced differences in the *I*(*V*) curves at very low energies are traced back to the unoccupied electronic structure of the differently oriented RuO_2 crystallites. Finally, this combined experimental and theoretical *I*(*V*)-LEEM approach allows us to follow the nucleation, growth, and coalescence of different faces of the same nanocrystalline oxide in real-time, thus providing novel and unique insights into the atomic structure and morphology of multicomponent material systems on the few nanometer scale and enabling real-time kinetic studies of dynamic processes in complex catalytic materials under reaction conditions.

METHODS

Low-Energy Electron Microscopy. The experiments were performed in a commercial Elmitec LEEM III system installed at the University of Bremen, Germany, and operating at an electron energy of 20 keV and a vacuum base pressure in the low 10^{-10} Torr range. The Ru(0001) single crystal (Mateck) was cleaned *ex situ* and *in situ* using well-tested procedures, involving repeated oxidation and high-temperature flash annealing as described elsewhere.[22] Emerging oxide nanostructures are systematically identified employing two complementary approaches: (i) microspot low-energy electron diffraction (μLEED) analysis of submicrometer sized surface phases with determination of the surface unit mesh and (ii) using their respective energy-dependent electron reflectivity *R*(*E*) spectra, also known as intensity−voltage (*I*(*V*)) curves of the reflected beam.[23]

***Ab Initio* Very-Low-Energy Electron Diffraction Calculations.** The analysis of the electron reflectivity of the three RuO_2 surfaces, (100), (101), and (110), is performed with an *ab initio* Bloch wave scattering theory. The LEED wave functions are calculated with the augmented-plane-waves-based embedding method:[24] in the interior of the crystal, they are represented by a linear combination of Bloch waves (which constitute the complex band structure, CBS) that smoothly and continuously matches a variational solution of the Schrödinger equation in the selvage region. This method fully takes into account the realistic crystal potential both in the bulk and at the surface, which is obtained self-consistently within the local density approximation of the

density functional theory. The inelastic scattering is taken into account by the optical potential (imaginary potential, iV_i added to the Hamiltonian in the crystal half-space), which is spatially constant in the crystal and zero in the vacuum half-space. Further details regarding the interpretation of the normal-incidence reflectivity spectra of the (100), (101), and (110) faces of RuO_2 is provided in Section S3 of the Supporting Information. For an application to oxygen (sub)monolayers on Ru(0001), the reader is referred to our previous work.[14]

Conflict of Interest: The authors declare no competing financial interest.

Acknowledgment. Technical assistance by Axel Meyer and Torben Rohbeck (University of Bremen) is gratefully acknowledged. This work was supported by the Spanish Ministry of Economy and Competitiveness MINECO (Project No. FIS2013-48286-C2-1-P).

Supporting Information Available: Real-time LEEM movie showing the oxidation of the Ru(0001) surface during exposure to molecular oxygen at 780 K, simulated μLEED patterns for the different RuO_2 faces, and a detailed comparison of the calculated $R(E)$ spectra to the complex band structures of the individual oxide faces. The Supporting Information is available free of charge on the ACS Publications website at DOI: 10.1021/acsnano.5b03393.

Note Added after ASAP Publication: This paper published ASAP on July 21, 2015. An author affiliation was corrected and the revised version was reposted on July 23, 2015.

REFERENCES AND NOTES

1. Over, H. Surface Chemistry of Ruthenium Dioxide in Heterogeneous Catalysis and Electrocatalysis: From Fundamental to Applied Research. *Chem. Rev.* **2012**, *112*, 3356–3426.
2. Lundgren, E.; Gustafson, J.; Resta, A.; Weissenrieder, J.; Mikkelsen, A.; Andersen, J. N.; Köhler, L.; Kresse, G.; Klikovits, J.; Biederman, A.; et al. The Surface Oxide as a Source of Oxygen on {Rh(111)}. *J. Electron Spectrosc. Relat. Phenom.* **2005**, *144-147*, 367–372.
3. Weaver, J. F. Surface Chemistry of Late Transition Metal Oxides. *Chem. Rev.* **2013**, *113*, 4164–4215.
4. Waddill, G.; Ozturk, O. Epitaxial Growth of Iron Oxide Films on Ag(111). *Surf. Sci.* **2005**, *575*, 35–50.
5. Lübbe, M.; Gigler, A. M.; Stark, R. W.; Moritz, W. Identification of Iron Oxide Phases in Thin Films Grown on Al_2O_3(0001) by Raman Spectroscopy and X-ray Diffraction. *Surf. Sci.* **2010**, *604*, 679–685.
6. Weiss, W.; Ranke, W. Surface Chemistry and Catalysis on Well-Defined Epitaxial Iron-Oxide Layers. *Prog. Surf. Sci.* **2002**, *70*, 1–151.
7. Over, H.; Kim, Y. D.; Seitsonen, A. P.; Wendt, S.; Lundgren, E.; Schmid, M.; Varga, P.; Morgante, A.; Ertl, G. Atomic-Scale Structure and Catalytic Reactivity of the RuO_2(110) Surface. *Science* **2000**, *287*, 1474–1476.
8. Herd, B.; Knapp, M.; Over, H. Atomic Scale Insights into the Initial Oxidation of Ru(0001) Using Molecular Oxygen: a Scanning Tunneling Microscopy Study. *J. Phys. Chem. C* **2012**, *116*, 24649–24660.
9. Böttcher, A.; Krenzer, B.; Conrad, H.; Niehus, H. Mesoscopic-Scale Growth of Oxygen-Rich Films on Ru(0001) Investigated by Photoemission Electron Microscopy. *Surf. Sci.* **2002**, *504*, 42–58.
10. Böttcher, A.; Starke, U.; Conrad, H.; Blume, R.; Niehus, H.; Gregoratti, L.; Kaulich, B.; Barinov, A.; Kiskinova, M. Spectral and Spatial Anisotropy of the Oxide Growth on Ru(0001). *J. Chem. Phys.* **2002**, *117*, 8104–8109.
11. Blume, R.; Niehus, H.; Conrad, H.; Böttcher, A.; Aballe, L.; Gregoratti, L.; Barinov, A.; Kiskinova, M. Identification of Subsurface Oxygen Species Created During Oxidation of Ru(0001). *J. Phys. Chem. B* **2005**, *109*, 14052–14058.
12. Blume, R.; Hävecker, M.; Zafeiratos, S.; Teschner, D.; Kleimenov, E.; Knop-Gericke, A.; Schlögl, R.; Barinov, A.; Dudin, P.; Kiskinova, M. Catalytically Active States of Ru(0001) Catalyst in CO Oxidation Reaction. *J. Catal.* **2006**, *239*, 354–361.
13. He, Y. B.; Knapp, M.; Lundgren, E.; Over, H. Ru(0001) Model Catalyst under Oxidizing and Reducing Reaction Conditions: *In-Situ* High-Pressure Surface X-ray Diffraction Study. *J. Phys. Chem. B* **2005**, *109*, 21825–21830.
14. Krasovskii, E. E.; Höcker, J.; Falta, J.; Flege, J. I. Surface Resonances in Electron Reflection from Overlayers. *J. Phys.: Condens. Matter* **2015**, *27*, 035501.
15. Further details regarding the relation of the calculated $R(E)$ spectra to the complex band structures of the individual oxide phases are found in Section S3 of the Supporting Information.
16. Teschner, D.; Farra, R.; Yao, L.; Schlögl, R.; Soerijanto, H.; Schomäcker, R.; Schmidt, T.; Szentmiklósi, L.; Amrute, A. P.; Mondelli, C.; et al. An Integrated Approach to Deacon Chemistry on RuO_2-based Catalysts. *J. Catal.* **2012**, *285*, 273–284.
17. Wang, T.; Jelic, J.; Rosenthal, D.; Reuter, K. Exploring Pretreatment−Morphology Relationships: *Ab Initio* Wulff Construction for RuO_2 Nanoparticles under Oxidising Conditions. *ChemCatChem* **2013**, *5*, 3398–3403.
18. Kim, Y. D.; Schwegmann, S.; Seitsonen, A. P.; Over, H. Epitaxial Growth of RuO_2(100) on Ru(10$\bar{1}$0): Surface Structure and Other Properties. *J. Phys. Chem. B* **2001**, *105*, 2205–2211.
19. Lin, W. F.; Zei, M. S.; Kim, Y. D.; Over, H.; Ertl, G. Electrochemical *versus* Gas-Phase Oxidation of Ru Single-Crystal Surfaces. *J. Phys. Chem. B* **2000**, *104*, 6040–6048.
20. He, Y. B.; Stierle, A.; Li, W. X.; Farkas, A.; Kasper, N.; Over, H. Oxidation of Ir(111): From O−Ir−O Trilayer to Bulk Oxide Formation. *J. Phys. Chem. C* **2008**, *112*, 11946–11953.
21. Chung, W.-H.; Tsai, D.-S.; Fan, L.-J.; Yang, Y.-W.; Huang, Y.-S. Surface Oxides of Ir(111) Prepared by Gas-Phase Oxygen Atoms. *Surf. Sci.* **2012**, *606*, 1965–1971.
22. Madey, T. E.; Engelhardt, H. A.; Menzel, D. Adsorption of Oxygen and Oxidation of CO on the Ruthenium (001) Surface. *Surf. Sci.* **1975**, *48*, 304–328.
23. Flege, J. I.; Krasovskii, E. E. Intensity-Voltage Low−Energy Electron Microscopy for Functional Materials Characterization. *Phys. Status Solidi RRL* **2014**, *8*, 463–477.
24. Krasovskii, E. E. Augmented-Plane-Wave Approach to Scattering of Bloch Electrons by an Interface. *Phys. Rev. B: Condens. Matter Mater. Phys.* **2004**, *70*, 245322.